On the Formation of Eutectics in Variations of the $Al_{10}Co_{25}Cr_8Fe_{15}Ni_{36}Ti_6$ Compositionally Complex Alloy

A. M. Manzoni, F. Dubois, M. S. Mousa, C. von Schlippenbach, D. M. Többens, Y. Yesilcicek, E. Zaiser, R. Hesse, S. Haas & U. Glatzel

Metallurgical and Materials Transactions A

ISSN 1073-5623

Metall Mater Trans A
DOI 10.1007/s11661-020-06091-7

Springer

On the Formation of Eutectics in Variations of the $Al_{10}Co_{25}Cr_8Fe_{15}Ni_{36}Ti_6$ Compositionally Complex Alloy

A.M. MANZONI, F. DUBOIS, M.S. MOUSA, C. VON SCHLIPPENBACH, D.M. TÖBBENS, Y. YESILCICEK, E. ZAISER, R. HESSE, S. HAAS, and U. GLATZEL

Superalloy inspired $Al_{10}Co_{25}Cr_8Fe_{15}Ni_{36}Ti_6$ compositionally complex alloy is known for its γ-γ' microstructure and the third Heusler phase. Variations of this alloy, gained by replacing 0.5 or 1 at. pct Al by the equivalent amount of Mo, W, Zr, Hf or B, can show more phases in addition to this three-phase morphology. When the homogenization temperature is chosen too high, a eutectic phase formation can take place at the grain boundaries, depending on the trace elements: Mo and W do not form eutectics while Hf, Zr and B do. In order to avoid the eutectic formation and the potential implied grain boundary weakening, the homogenization temperature must be chosen carefully by differential scanning calorimetry measurements. A too low homogenization temperature, however, could impede the misorientation alignment of the dendrites in the grain. The influence of grain boundary phases and incomplete dendrite re-orientation are compared and discussed.

https://doi.org/10.1007/s11661-020-06091-7

I. INTRODUCTION

AFTER two decades of research on high entropy alloys (HEA) and compositionally complex alloys (CCA), several procedures have been cornered as being essential for a good understanding of the material inherent properties. One of the most important ones in cast alloys is probably the adequate homogenization of the alloy.[1] Removing the compositional variances that are induced by the type of casting and parameters such as cast size, cooling rate, contact to the crucible and many others allows for a reproducibility of the material by other research groups and for pushing the alloy closer to the, alas, hardly reachable thermodynamic equilibrium. This procedure has been used for centuries in all types of alloys and is just as valid in single-phase HEA and multi-phase CCA, which add a challenge to the finding of the correct homogenization parameters by their high number of elements.

During the last few years, the authors' group has found the $Al_{10}Co_{25}Cr_8Fe_{15}Ni_{36}Ti_6$ CCA to be of high interest for a potential application at around 700 °C.[2–5] Optimizing parameters have been predicted by ThermoCalc[6] using the TTNI7 database,[7] tested in numerous casting and heat treatment experiments until the best parameters had been found to be 1220 °C 20 hours for homogenization. Once the alloy reached its best microstructural and mechanical properties, another path for further improvement was chosen, *i.e.* by the addition of trace elements that would push the properties beyond the base alloy's. Besides the expected change in mechanical properties, a change in optimizing parameters was expected as well. It was quickly found that the homogenization temperature of 1220 °C, which was used for the base alloy, was not adequate for many alloy variations because of a eutectic formation of two or three phases, subsequently called the eutectic or the eutectic phases for simplicity, both at the grain boundaries and inside the grains. Unlike in alloys designed for consisting entirely of eutectic phases,[8] which can provide good combinations of strength and ductility,[9] an uncontrolled local formation of eutectic phases is not desirable. Unwanted phases at the grain boundaries can destabilize the latter, which is particularly harmful in high temperature applications and must be avoided.

A.M. MANZONI is with the Bundesanstalt für Materialforschung und -prüfung, Unter den Eichen 87, 12203 Berlin, Germany and also with the Helmholtz-Zentrum Berlin für Materialien und Energie GmbH, Hahn-Meitner-Platz 1, 14109 Berlin, Germany. Contact e-mail: anna_manzoni@gmx.net F. DUBOIS, C. VON SCHLIPPENBACH, and D.M. TÖBBENS are with the Helmholtz-Zentrum Berlin für Materialien und Energie GmbH; M.S. MOUSA is with the Department of Physics, Mu'tah University, Al-Karak 61710, Jordan. Y. YESILCICEK and R. HESSE are with the Bundesanstalt für Materialforschung und -prüfung; E. ZAISER is with the Helmholtz-Zentrum Berlin für Materialien und Energie GmbH and also with the Technical University Berlin, Straße des 17. Juni 135, 10623 Berlin, Germany. S. HAAS and U. GLATZEL are with the Metals and Alloys, University Bayreuth, Prof.-Rüdiger-Bormann-Str. 1, 95447 Bayreuth, Germany.

Manuscript submitted July 3, 2020; accepted October 29, 2020.

Published online: 18 November 2020

Thus, we have combined a series of methods for predicting, characterizing and particularly avoiding the eutectic formation and at the same time ensuring a sufficient homogenization process all the same for a successful subsequent annealing and application.

II. MATERIALS AND METHODS

All alloys were prepared from pure elements of 99.999 pct purity. They were melted together in a vacuum induction furnace, re-melted three times to ensure homogeneity and cooled in a water-cooled Cu crucible to form ingots of 20 to 25 g. They were then homogenized in an Ar atmosphere at different times and temperatures and cooled down in the furnace. Six alloys, *i.e.* the base alloy $Al_{10}Co_{25}Cr_8Fe_{15}Ni_{36}Ti_6$ and five of its modifications are being compared in this manuscript. The alloys' nominal compositions and their homogenization parameters are summarized in Table I. For the sake of brevity, they will be named after their trace element, *e.g.* "alloy with Hf" in case of the $Al_{9.5}Co_{25}Cr_8Fe_{15}Ni_{36}Ti_6Hf_{0.5}$ alloy.

Samples used for X-ray diffraction (XRD) experiments underwent a subsequent heat treatment of 900 °C 50 hours, which promotes the formation of the γ' particles, allowing them to gain their optimum shape. It has no detectable influence on the other phases.

Phase diagrams were calculated via the CALPHAD method, using ThermoCalc[6] and the database TTNi7.[7]

Samples for optical microscopy (OM), scanning electron microscopy (SEM) and synchrotron XRD were prepared by mechanical grinding and polishing, down to a final polishing step using a 50 nm sized colloidal Si suspension.

The SEM used in this study was a Zeiss Leo 1530 operated at 30 kV for imaging. It is equipped with a detector for energy dispersive X-ray spectroscopy (EDS) and the voltage used for EDS was 16 kV, except for the alloy with Zr where the voltage was only 5 kV. The detector used was a secondary electron (SE) detector.

DSC measurements were carried out on as-cast samples in two different instruments: (1) a DSC 404 C Pegasus (base alloy and alloys with Hf, Zr and Mo) and (2) a DSC STA 449 Jupiter F3 (alloys with B and W), both from the company Netzsch, using a heating and cooling rate of 20 K/min. Measurements after homogenization and annealing were carried out as well but are not shown here.

XRD observations were carried out at the KMC-2 beamline at BESSY II in Berlin.[10] As a preparation for these measurements, the polycrystalline samples were first observed by optical microscopy and large grains were marked with a permanent marker. The orientation of these grains was analysed by Laue diffraction so that samples could be mounted pre-oriented at the synchrotron. For each alloy, one grain and two different planes were observed, either (300) and (200) or (110) and (220).

For intensity reasons, the spot size used during the synchrotron measurements was on average 0.5 × 0.5 mm^2. Depending on the analysed grain's orientation in space, the incident angle (typically between 8 and 15 deg), the surface that is hit by the beam and the penetration depth are different, but the interaction volume is around 2000 μm^3, which is large for XRD experiments but small compared to preceding neutron diffraction experiments on superalloys.[11,12] Radiation energy of 8040 eV, corresponding to the wavelength of 0.15406 nm of Cu $K\alpha_1$, was used. The diffraction station at KMC-2 is a si-circle goniometer in ψ geometry. The complete setup of the beamline has been shown in a previous work.[4] Two angles are of major importance in this study: the angle chi, which is perpendicular to the plane set up by the source—sample—detector, or by θ to 2θ, and the angle 2θ from which the lattice parameter can be determined. The detector gives information in 2D and covers a range of about 14 deg in both 2θ and chi. The Origin® software[13] was used for fitting the peaks from the different dendrites.

III. RESULTS AND DISCUSSION

A. *Microstructure: Overview and the Eutectic Phase Formation*

Figure 1 shows two overview micrographs of two alloys, *i.e.* (a) the alloy with Zr after too high homogenization and (b) the alloy with B in the as-cast state. Grain sizes after casting can reach up to 1 mm, as shown in Figure 1(a), and no investigated heat treatment influences the grain sizes. These large grains are well suited for synchrotron diffraction measurements, shown in Part 4 below. Dendrite growth can be best observed in the as-cast state (Figure 1(b)). It is similar in all investigated alloys, as all of them have been cast the same. The cooling in the water-cooled Cu crucible leads to primary dendrite arm spacings λ_1 of about 80 μm and a cross section of about 3200 μm^2 (see highlighted dendrite in Figure 1(b)). This is rather small compared to former studies on the influence of cooling on the dendrite size in a Ni-based superalloy, in which the primary dendrite arm spacings were up to 290 μm.[14] In the upper grain, the view is perpendicular to the primary dendrite growth and shows no misorientation between them, but this can vary from one grain to another.

The use of the homogenization parameters developed for the base alloy lead to similar results in the alloys with Mo and W: all dendritic segregation was removed, and no microstructural features are visible at the μm scale, except for some porosities and nitrides (see Figure 2(a) and (c)).

However, the same homogenization temperature leads to a very different response in the alloys with Hf, Zr and B, as is shown in Figures 3(a) through (c), respectively. The grain boundaries are no longer clean but filled with eutectic phases. In addition, there are several round shaped phases inside the grains. A zoom on these by SEM, see *e.g.* Figure 3(d) for the alloy with Zr, reveals a eutectic formation as well. The use of the

Table I. Nominal Compositions of the Investigated Alloys (in At. Pct) and Their Homogenization Parameters

Alloy [At. Pct]	Homogenization	References
Base alloy $Al_{10}Co_{25}Cr_8Fe_{15}Ni_{36}Ti_6$	1220 °C 20 hours	2
$Al_9Co_{25}Cr_8Fe_{15}Ni_{36}Ti_6$**Mo$_1$**	1220 °C 20 hours	3
$Al_9Co_{25}Cr_8Fe_{15}Ni_{36}Ti_6$**W$_1$**	1220 °C 20 hours	this work
$Al_{9.5}Co_{25}Cr_8Fe_{15}Ni_{36}Ti_6$**Hf$_{0.5}$**	1130 °C 20 hours	3
$Al_{9.5}Co_{25}Cr_8Fe_{15}Ni_{36}Ti_6$**Zr$_{0.5}$**	1100 °C 200 hours	this work
$Al_{9.5}Co_{25}Cr_8Fe_{15}Ni_{36}Ti_6$**B$_{0.5}$**	1160 °C 160 hours (note that this homogenization temperature is too high)	this work

The bold numbers highlight the additional element that changes from one alloy to the next.

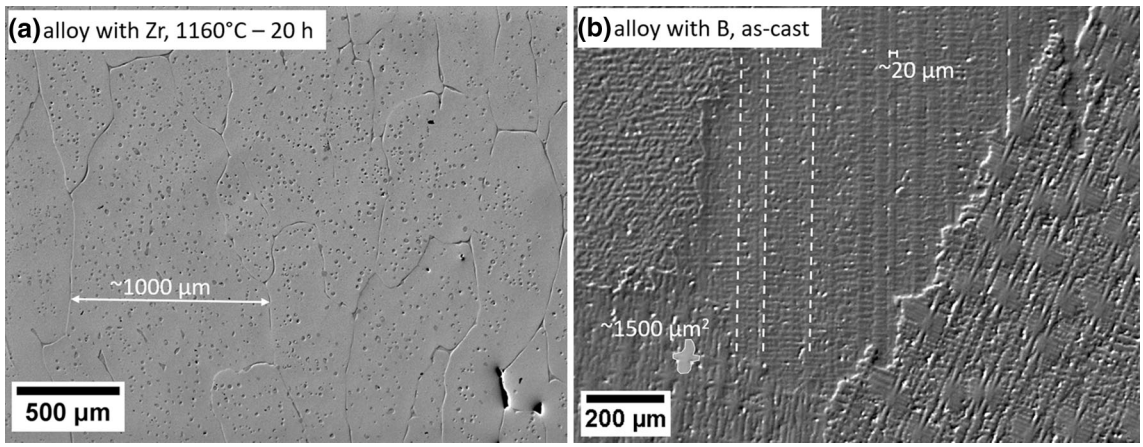

Fig. 1—Optical micrograph showing examples of (*a*) the grain size and (*b*) the dendrite size and primary dendrite arm orientations in the poly crystalline samples.

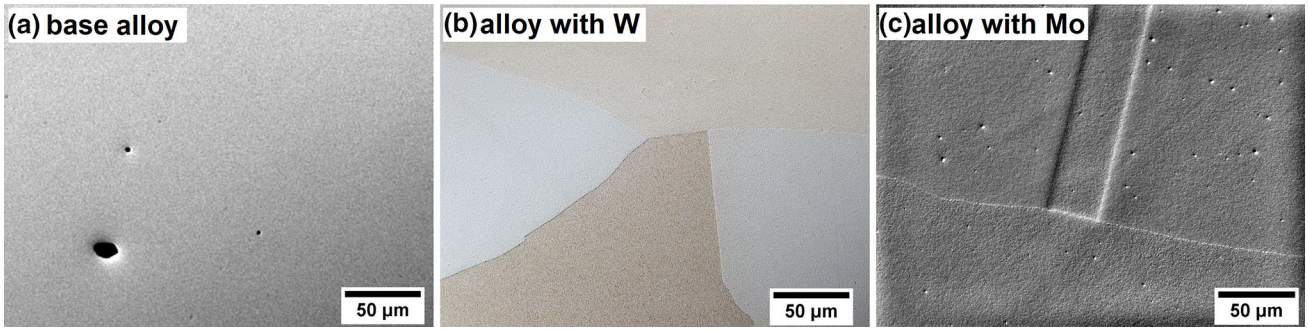

Fig. 2—Optical micrographs of (*a*) the base alloy, (*b*) the alloy with W and (*c*) the alloy with Mo after homogenization at 1220 °C 20 hours.

EDS-detector allows for elemental information in these formations. In all cases, the eutectic forms preferentially in places with higher energy such as the grain boundaries or next to the Heusler phases. In all alloys, the new phase is rich in the trace element.

There is a difference in the formation of the eutectic region: in the alloys with Zr and with B, the eutectic is binary, while in the alloy with Hf it is ternary. In the alloy with Zr the eutectic combines the Zr rich phase with the Heusler phase; in the B rich alloy it combines TiB_2 with the γ phase, and in the Hf rich alloy we can see the Heusler phase, γ' and the Hf phase all intertwined. Compositions of the eutectic phases as determined by SEM-EDS are summarized in Table II, bearing in mind that EDS is insufficient for light elements, especially B. Nevertheless, a qualitative trend can be observed.

At a higher magnification, all alloys reveal a γ-γ' morphology, as has been shown before for the base alloy and the alloy with Mo and Hf.[2–4,15] As these phases are not relevant for this study, they will not be presented in further detail.

B. *Thermic Response: the Eutectic Peak*

Figure 4(a) shows the heating curves up to the onset of the melting peak in the DSC responses of the base alloy and its five variations. The alloys can be separated into two groups:

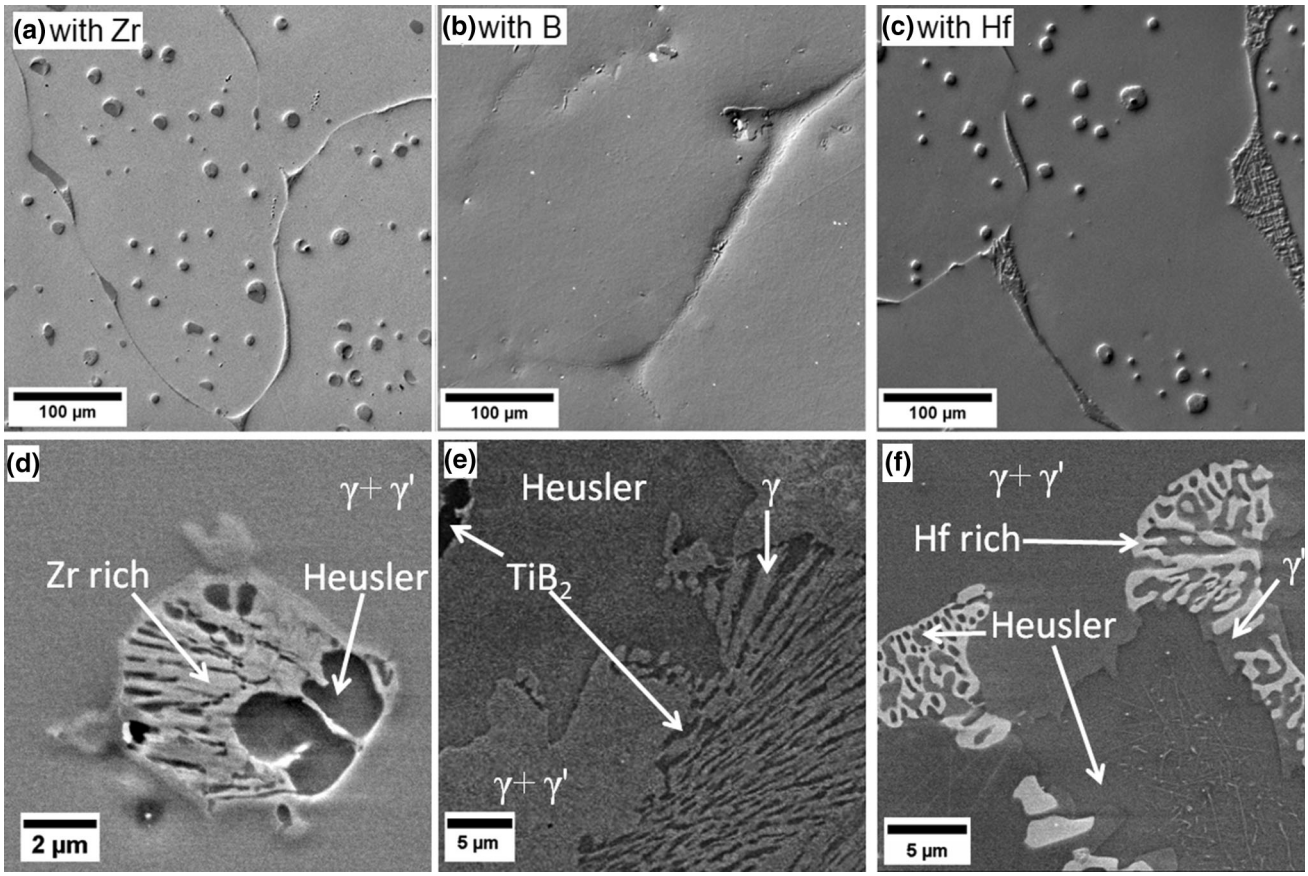

Fig. 3—Overview over the three alloys with Zr (*a* and *d*), B (*b* and *e*) and Hf (*c* and *f*), which have been heat treated at too high temperature, *i.e.* 1220 °C: upper line: OM at low magnification showing the eutectic morphology that can be seen at the grain boundaries and inside the grains, around the Heusler phase. Lower: SEM micrographs using a higher magnification of the eutectic regions and annotation of the phases. Note that the high magnification image of the alloy with B was obtained at 1160 °C 160 hours.

– The base alloy and the variations with Mo and W have a smooth response without any additional peak.
– The alloys with Hf, Zr and B show peaks of different magnitudes between about 1130 °C (Zr) and 1165 °C (B). These correspond to the formation temperature of the eutectic phases.

Figure 4(b) shows the entire cooling curves, including the solidification peak (except for the base alloy), which induces a larger heat range in the *y*-axis. These curves are not used for the determination of the eutectic peaks.

Eutectic DSC responses have been shown before in the alloy family that has been called "eutectic high entropy alloys (EHEA)", in alloys such as AlCoCrFeNi$_{2.1}$[16] or CoCrFeNi$_2$-based alloys with Zr, Nb, Hf or Ta.[17] In that family, the alloys solidify from the melt directly into a two-phase eutectic microstructure. The present alloys with the eutectic peaks, *i.e.* the ones with Hf, Zr and B, are better compared *e.g.* to the CoCrFeNiTa$_{0.4}$ alloy presented by Jiang *et al.*[18] Here, the eutectic formation occurs at a temperature below the general melting point of the alloy: at high temperature there is a stable phase, but the local deviations from the stoichiometry, positioned at the grain boundaries and next to the Heusler phase, create regions in which a eutectic formation is made possible.

The step formation between 1075 °C and 1105 °C, best visible at about 1075 °C in the alloy with Mo, is attributed to the dissolution of the γ' phase. They exist in all alloys but are more flattened and thus less visible in the base alloy and the alloys with W and B. These step formations can be reinforced by using annealed samples instead of as-cast samples (not shown here), but as this is not the focus of this work, it will not be presented any further.

C. *Calculations Using ThermoCalc*

Figure 5 shows the calculations of the six alloy variants' phase diagrams using ThermoCalc[6] and the TTNI7 database.[7] The phase diagram calculation of the base alloy has been shown in a previous work[5] and adapted here.

None of the six variations shows a eutectic, but this is not surprising as the local concentration around the eutectic formations varies greatly from the nominal one that has been used for the CALPHAD calculation. Temperatures below 600 °C are not considered in the current considerations because it is too difficult to reach

Table II. Compositions in the Eutectic Phases as Determined by SEM-EDS (in At. Pct)

	Al	Co	Cr	Fe	Ni	Ti	Zr	B	Hf	C, N, O
$Al_{9.5}Co_{25}Cr_8Fe_{15}Ni_{36}Ti_6\mathbf{Zr_{0.5}}$										
Heusler	17 ± 2	22 ± 1	5 ± 3	8 ± 1	35 ± 2	9 ± 1	1 ± 1	—	—	bal.
Zr rich	7 ± 1	24 ± 1	8 ± 2	9 ± 1	36 ± 2	6 ± 0	7 ± 1	—	—	bal.
$Al_{9.5}Co_{25}Cr_8Fe_{15}Ni_{36}Ti_6\mathbf{B_{0.5}}$										
γ matrix	5 ± 1	26 ± 3	8 ± 1	14 ± 2	28 ± 3	11 ± 1	—	3 ± 1	—	bal.
TiB_2	1 ± 0	28 ± 3	11 ± 1	10 ± 2	13 ± 2	28 ± 2	—	10 ± 2	—	bal.
$Al_{9.5}Co_{25}Cr_8Fe_{15}Ni_{36}Ti_6\mathbf{Hf_{0.5}}$										
Heusler	21 ± 1	20 ± 1	3 ± 0	8 ± 1	34 ± 1	11 ± 1	—	—	2 ± 1	bal.
γ'	9 ± 1	20 ± 1	4 ± 1	8 ± 3	46 ± 2	10 ± 0	—	—	3 ± 1	bal.
Hf rich	5 ± 2	22 ± 0	2 ± 0	7 ± 0	44 ± 2	6 ± 1	—	—	15 ± 0	bal.

The bold numbers highlight the additional element that changes from one alloy to the next.
Errors are determined during the measurement.

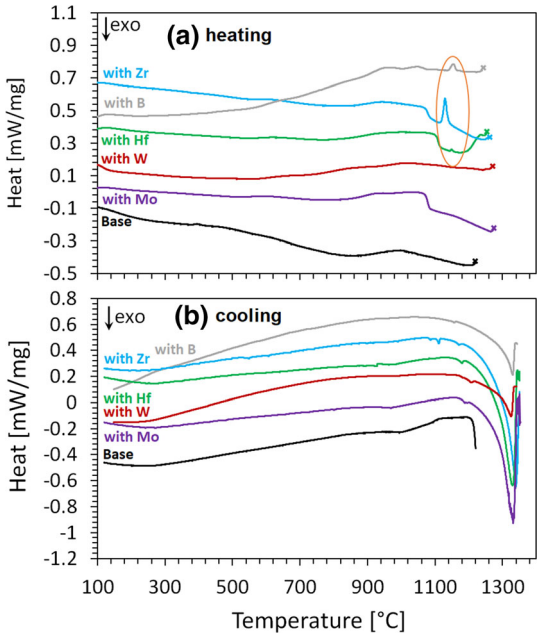

Fig. 4—Extracts from the DSC curves of all six alloys, (*a*) heating and (*b*) cooling. The orange ellipse highlights the regions where eutectic peaks can be seen, *i.e.* in the alloys with B, Zr and Hf. Crosses at the end of the curves symbolize the onset of the melting peak (Color figure online).

thermodynamic equilibrium in experiments at these lower temperatures. The alloys with Mo, Hf and W show a single-phase region at high temperature, just like the base alloy. The variations with B and Zr show at least one additional phase. All of them predict the formation of B2 structured NiAl. This is never observed experimentally, but instead an $L2_1$ structured Heusler phase is present in all alloys, albeit a close relationship to B2 cannot be denied. The Heusler phase can be dissolved above 1160 °C—it is not detectable in the homogenized states of the base alloy and the variations with W and Mo, which are homogenized at 1220 °C. Note that it remains detectable in the alloys with Hf, B and Zr inappropriately homogenized at 1220 °C 20 hours. These trace elements seem to stabilize the domain of existence of the Heusler phase towards higher temperatures.

D. *Influences of the Enforced Lower Homogenization Temperature on the Microstructure and Mechanical Properties*

A comparison of the broad scale microstructural aspects is shown exemplarily for the alloy with Hf in Figure 6. A homogenization at 1130 °C, shown in Figure 6(a), reveals meandering grain boundaries that are often fixed in place by the Heusler phase (dark grey). Remainders of the dendritic solidification can be clearly seen, and it is suggested that a dendritic mosaicity is retained within the individual grains. A homogenization at 1220 °C, *i.e.* 90 °C higher, shown in (Figure 6(b)), results in fluid, widely straight grain boundaries with no more traces of the dendritic solidification.

This reflection on the presence of differently oriented dendrites in alloys with lower homogenization temperatures has been confirmed by XRD observations at the KMC-2 beamline at BESSY-2. Note that the large spot size of 0.5 × 0.5 mm^2 and a rough penetration depth of about 2 μm (calculated for Cu $K\alpha_1$, the observed alloy and the sample angle) can give information on several hundred dendrites in one grain. Figure 7 shows exemplarily the XRD response in two alloys that have been homogenized at 1220 °C (Figure 7(a)) and 1100 °C (Figure 7(b)). The horizontal axis covers the 2θ range of 14 deg while the vertical axis covers the chi range, also of 14 deg. Remember that the chi axis is perpendicular to the plane set up by the source—sample-detector. Observations with a 1D detector fixed in this plane would not be able to give information on this particular angular response.

In both figures a spread of the peak along 2θ can be observed. This corresponds to the peaks of the γ' and γ phases, as has been shown in previous studies.[4] However, the alloy with W in (a), homogenized at 1220 °C, shows only one response (c) in the chi axis, while the alloy with Zr in (b), homogenized at 1100 °C, shows four different responses, which can be attributed to four different dendrites. An analysis of their positions (d) shows that they are separated by about 0.2 deg from the next dendrite. This means that at the given sample angle there

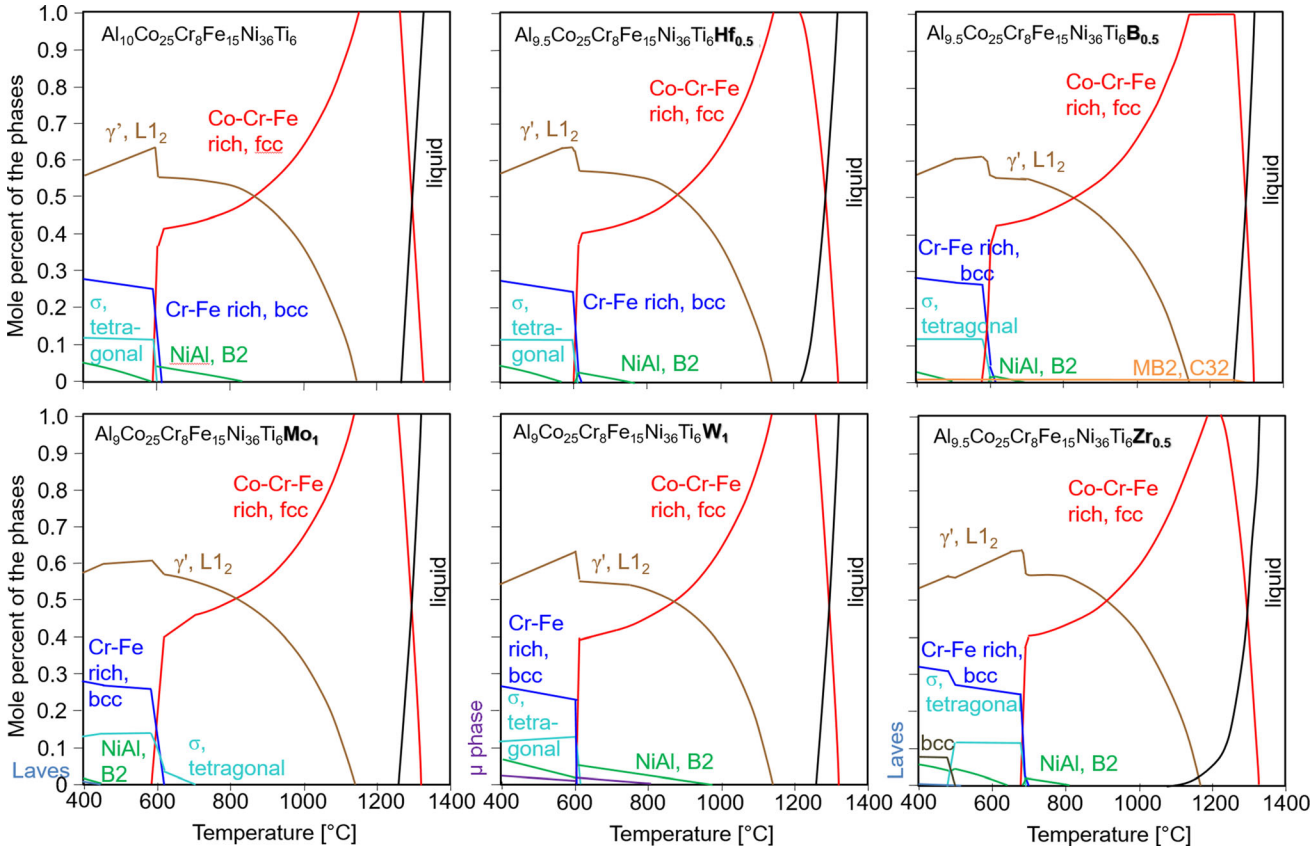

Fig. 5—Calculations of the phase diagrams of the base alloy and its variants using ThermoCalc[6] and the TTNI7 database.[7]

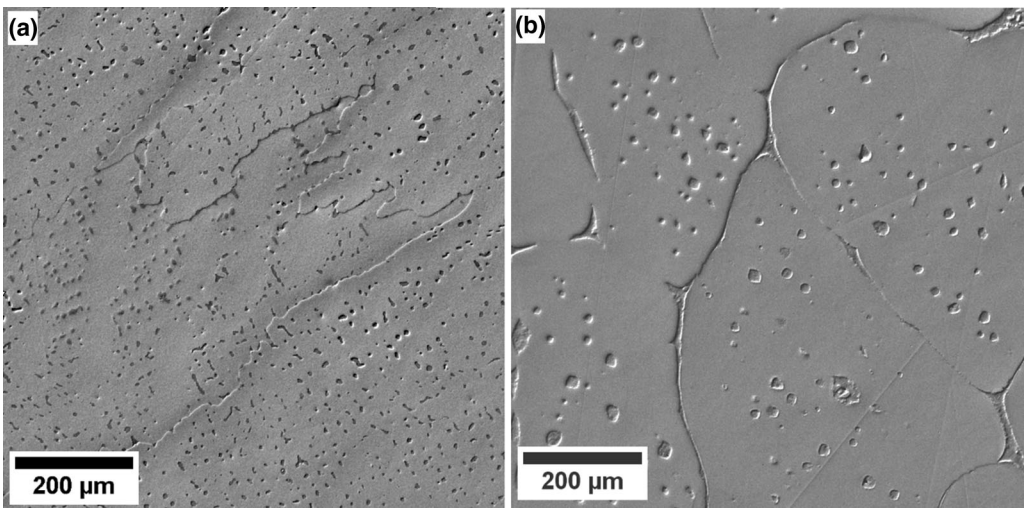

Fig. 6—Optical micrographs of two different homogenization in the alloy with Hf: (*a*) at 1130 °C 20 hours, (*b*) at 1220 °C 20 hours.

are at least four different dendrites within the excited interaction volume in the observed grain.

The homogenization at higher temperature (1220 °C) in the alloy with W made it possible to reduce the dendrite misorientation in the observed grain. This was not possible at the lower homogenization temperature (1100 °C) in the alloy with Zr.

While a complete removal of dendritic mosaicity might seem preferable on a first idea, it has long been accepted in commercial superalloys that a deviation of several degrees is tolerable for application. Single crystal CMSX-4 may grow up to 15 deg astray from a perfect [100] growth direction.[19] Observations in a directionally solidified CMSX-4 showed a bending of 1.7 deg

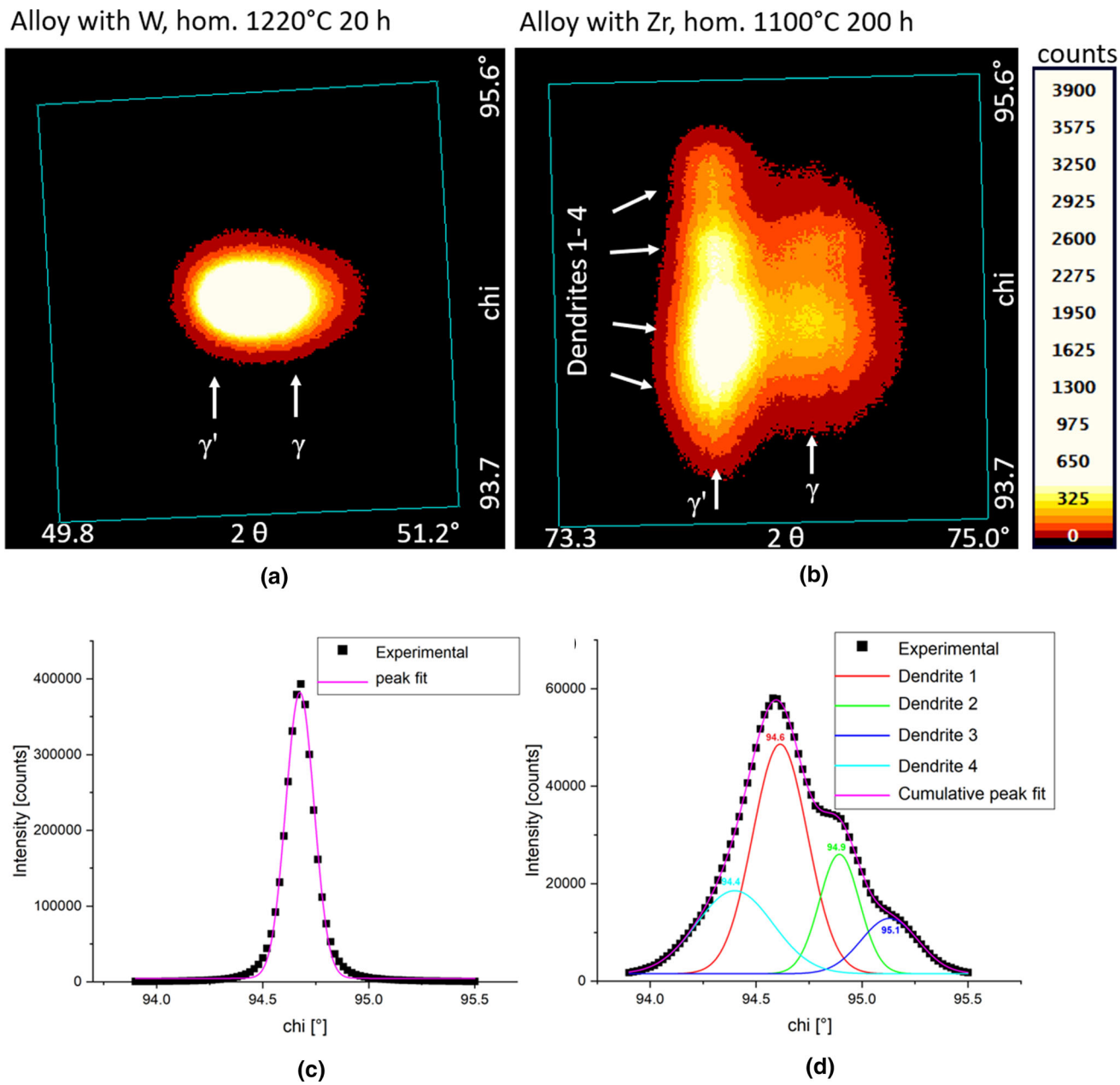

Fig. 7—XRD peaks as determined with the 2D detector at the beamline KMC-2: (*a*) the alloy with W, homogenized at 1220 °C 20 hours, showing one single position for the 200 peaks set up by γ and γ'; and (*b*) the alloy with Zr, homogenized at 1100 °C 200 hours, showing the response of the 220 peaks of γ' and sometimes γ located in four different dendrites; (*c*) integration over 2θ showing the response of one single dendrite in the alloy with W; (*d*) integration over 2θ showing the response of four dendrites in the alloy with Zr.

over a length of 25 mm and a misorientation of up to 3 deg between dendrites.[20] These misorientation values do not restrain the alloy from showing some of the best mechanical properties in the high temperature alloy family and from being widely used.

Similar observations can be made within the CCA family presented in this work. A previous study pointed out the good mechanical properties of the alloy with Hf,[3] an alloy that has been homogenized at 1130 °C. Even though it shows a remaining mosaicity, its properties are better than those of the base alloy and of the alloy with Mo, both homogenized at 1220 °C. It can thus be concluded that the lower homogenization temperature and the presence of misorientations between dendrites is not the most important criterion for good mechanical properties. Considering the detrimental effect of eutectic phases on grain boundary weakening at high temperature, the avoidance of their formation is to be preferred to the avoidance of dendrite misorientation.

IV. SUMMARY

Homogenization studies on the $Al_{10}Co_{25}Cr_8Fe_{15}Ni_{36}Ti_6$ base alloy and five variations revealed the

formation of eutectic phases when specific trace elements are added:

- Hf, Zr and B trace element cause a eutectic response at the grain boundaries and close to the Heusler phase, which could not be predicted by CALPHAD calculations and which forces the use of a lower homogenization temperature than what was determined in the base alloy.
- Trace elements Mo and W do not provoke a eutectic formation and thus their homogenization temperature is not changed.

Homogenization at high temperature, *i.e.* 1220 °C, reduces the spread of dendritic misorientation angles within the grains, while lower homogenization temperatures are less effective. However, as the angular spread is low in the investigated volume and less than what is acceptable in commercially used superalloys, this does not seem to be a major problem for the potential application of these alloys at high temperature. It is more important to avoid the formation of a weakening eutectic phase.

ACKNOWLEDGMENTS

The authors are grateful to the German Research foundation (DFG) for the financial support through MA7004/1-1 and -2 and GL181/50-1 and -2, and through the Priority Program SPP2006 "Compositionally Complex Alloys – High Entropy Alloys (CCA-HEA)". We thank HZB for the allocation of synchrotron radiation beamtime at beamline KMC-2. Many thanks to the Laue Camera at the HZB Quantum Material Core Lab and to Konrad Siemensmeyer for help with Laue experiments. Many thanks to Claudia Leistner for help with casting and to Christiane Förster for help with sample preparation. Thank you to Burkart Adamczyk, Sebastian Fiechter, Nora Wolff and Jan-Ekkehard Hoffmann for help with DSC experiments!

FUNDING

Open Access funding enabled and organized by Projekt DEAL.

OPEN ACCESS

REFERENCES

1. A.M. Manzoni and U. Glatzel: *Mater. Char.*, 2019, vol. 147, pp. 512–32.
2. H.M. Daoud, A.M. Manzoni, N. Wanderka, and U. Glatzel: *JOM*, 2015, vol. 67, pp. 2271–77.
3. S. Haas, A.M. Manzoni, F. Krieg, and U. Glatzel: *Entropy*, 2019, vol. 21, art. no. 169.
4. A.M. Manzoni, S. Haas, J.M. Yu, H.M. Daoud, U. Glatzel, H. Aboulfadl, F. Mücklich, R. Duran, G. Schmitz, D.M. Többens, S. Matsumura, F. Vogel, and N. Wanderka: *Mater. Char.*, 2019, vol. 154, pp. 363–76.
5. A.M. Manzoni, S. Singh, H.M. Daoud, R. Popp, R. Völkl, U. Glatzel, and N. Wanderka: *Entropy*, 2016, vol. 18, art. no. 104.
6. The Version TCCR, *ThermoCalc Software AB*, http://www.thermocalc.com, Stockholm, 2006.
7. Thermotech Ni-based Superalloys Database, TTNI7, *Thermo-Calc Software AB*, Stockholm, 2006.
8. I. Baker, M. Wu, and Z. Wang: *Mater. Char.*, 2019, vol. 147, pp. 545–57.
9. Y.P. Lu, X.Z. Gao, L. Jiang, Z.N. Chen, T.M. Wang, J.C. Jie, H.J. Kang, Y.B. Zhang, S. Guo, H.H. Ruan, Y.H. Zhao, Z.Q. Cao, and T.J. Li: *Acta. Mater.*, 2017, vol. 124, pp. 143–50.
10. Helmholtz-Zentrum Berlin für Materialien und Energie GmbH: *J. Large-Scale Res. Facil.*, 2016, vol. 2, art. no. A49.
11. U. Glatzel: *Scripta Met. Mater.*, 1994, vol. 31, pp. 291–96.
12. U. Glatzel and A. Muller: *Scripta Met. Mater.*, 1994, vol. 31, pp. 285–90.
13. Origin(Pro): *OriginLab Corporation*, Northampton, 2017.
14. A. Volek and R.F. Singer: *Superalloys 2004: Proceedings of the 10th Intenational Symposium of Superalloys,* Minerals, Metals and Materials Society.
15. A. Manzoni, S. Haas, H. Daoud, U. Glatzel, C. Förster, and N. Wanderka: *Entropy*, 2018, vol. 20, art. no. 646.
16. Y. Lu, Y. Dong, S. Guo, L. Jiang, H. Kang, T. Wang, B. Wen, Z. Wang, J. Jie, Z. Cao, H. Ruan, and T. Li: *Scientific Reports*, 2014, vol. 4, art. no. 6200.
17. Y. Lu, H. Jiang, S. Guo, T. Wang, Z. Cao, and T. Li: *Intermetallics*, 2017, vol. 91, pp. 124–28.
18. H. Jiang, K. Han, D. Qiao, Y. Lu, Z. Cao, and T. Li: *Mater. Chem. Phys.*, 2018, vol. 210, pp. 43–48.
19. K. Gancarczyk, R. Albrecht, H. Berger, D. Szeliga, A. Gradzik, and J. Sieniawski: *Metall. Mater. Trans. A*, 2017, vol. 48A, pp. 5200–05.
20. P. Hallensleben, F. Scholz, P. Thome, H. Schaar, I. Steinbach, G. Eggeler, and J. Frenzel: *Crystals*, 2019, vol. 9, art. no. 149.